



Metal cocatalyst mediated photocatalytic dehydrogenative-condensation and direct condensation cross-coupling of aniline and alcohol

Dongdong Lv^{a,c}, Yaru Li^{b,c,d}, Wei Qiao^e, Dongdong Zhang^e, Yuanqiang Mai^e, Nengjun Cai^e, Hongwei Xiang^{b,c,d}, Yongwang Li^{b,c}, Hans Niemantsverdriet^{c,f}, Weichang Hao^{a,*}, Ren Su^{c,e,**}

^a School of Physics and BUAA-UOW Joint research Center, Beihang University, Beijing 100191, China

^b State Key Laboratory of Coal Conversion, Institute of Coal Chemistry, CAS, Taiyuan 030001, China

^c SynCat@Beijing, Synfuels China Technology Co. Ltd., Leyuan South Street II, No.1, Yanqi Economic Development Zone C#, Huairou District, Beijing 101407, China

^d University of Chinese Academy of Sciences, Beijing 100049, China

^e Soochow Institute for Energy and Materials InnovationS (SIEMIS), Soochow University, China

^f SynCat@DIFFER, Syngaschem BV, 6336 HH Eindhoven, The Netherlands

ARTICLE INFO

Keywords:

Photocatalysis

Cross-coupling

Metal cocatalyst

Imines and secondary amines

Selectivity control

ABSTRACT

Cross coupling of aniline and alcohol for the synthesis of imine and secondary amines represents a highly atom efficient processes, yet achieving high selectivity requires specialized catalysts and harsh reaction conditions to avoid over-hydrogenation of as-produced imines and dehydrogenation of secondary amines. Here we employ metal cocatalysts to mediate photocatalytic activation of alcohols, thus separating the stepwise dehydrogenative-condensation process to imine and the direct condensation process to secondary amine. The Rh/TiO₂ promotes the photocatalytic dehydrogenation of alcohol into aldehyde and molecular hydrogen, resulting in rapid condensation of aldehyde with aniline to yield imine. In contrast, Fe/TiO₂ activates the alcohol mildly without forming aldehyde and hydrogen atoms under irradiation, allowing a direct dehydrative coupling of the activated alcohol with aniline to produce secondary amine. Both Rh/TiO₂ and Fe/TiO₂ photocatalysts show high performance in terms of conversion, selectivity, stability and a wide substrate scope, rendering the strategy promising for applications.

1. Introduction

Imines and secondary amines are important building blocks in organic synthesis for pharmaceutical, agricultural and biological applications [1–4]. Conventional syntheses of imines proceed via condensation of amines with aldehydes or ketones, which require dehydrating agents (i.e., strong acids and molecular sieves) and homogeneous catalysts to promote the elimination of water [5]. In the case of secondary amines, the major synthetic protocols are reductive amination of aldehydes/ketones and alkylation of primary amines with alkyl halides or transition metals [6–14]. These methods require harsh reducing reagents (i.e., sodium cyanoborohydride) or excess inorganic bases, which are neither incompatible with certain functional groups in the substrates nor desirable from the environmental point of view [15–19]. In addition, precise control of the selectivity to solely imine and secondary amine

remains as the major challenge. This normally requires delicate control over catalysts (i.e., Ru, Ir, and Pd based materials) and reaction conditions (i.e., solvent, pressure, and temperature) to manipulate the degree of dehydrogenation during the reaction [20,21]. Nevertheless, the formation of unavoidable by-products (i.e., salts, aldehydes, and ketones) calls for extra expenditures in separation processes [22].

Recently, the synthesis of imines and secondary amines via cross-coupling of primary amines with alcohols has attracted great interest [23–36]. The synthesis of imine undergoes an acceptorless dehydrogenative coupling process (ADC, top of Scheme 1), where the aldehyde intermediate is first produced by hydrogen abstraction from an alcohol and consequently been attacked by the nucleophilic amine via condensation with the liberation of H₂. To synthesize secondary amines, unsaturated imines are further hydrogenated via the so-called borrowing hydrogen (BH) process. The cross-coupling of primary

* Corresponding author.

** Corresponding author at: SynCat@Beijing, Synfuels China Technology Co. Ltd., Leyuan South Street II, No.1, Yanqi Economic Development Zone C#, Huairou District, Beijing 101407, China.

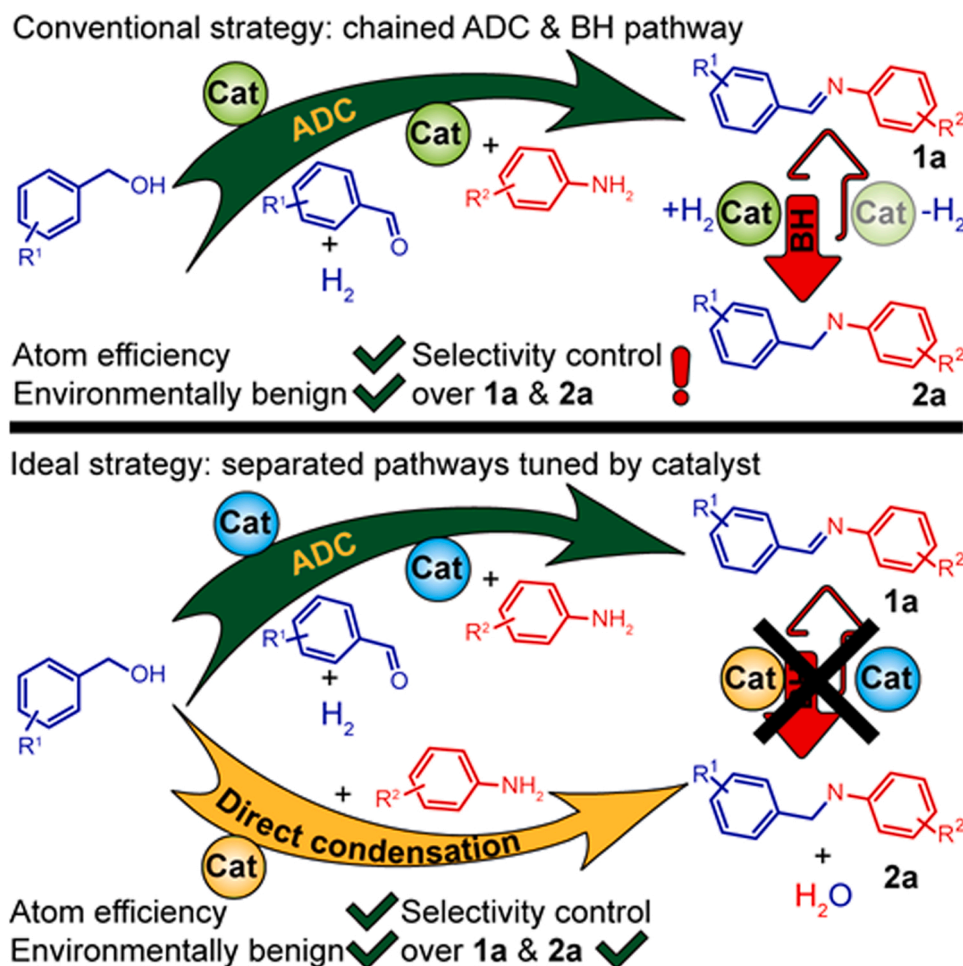
E-mail addresses: whao@buaa.edu.cn (W. Hao), suren@suda.edu.cn (R. Su).

<https://doi.org/10.1016/j.apcatb.2022.121264>

Received 11 January 2022; Received in revised form 18 February 2022; Accepted 25 February 2022

Available online 4 March 2022

0926-3373/© 2022 Elsevier B.V. All rights reserved.



Scheme 1. Pathways for the cross-coupling of aniline and alcohol. Above: conventional step-wise acceptorless dehydrogenative coupling (ADC) to imine and subsequent borrowing hydrogen (BH) paths to secondary amine; Below: ideal strategy with separated ADC and direct condensation.

amine and alcohol is a highly atom efficient and environmentally benign process that requires no hydrogen acceptor and produces less waste [23]. However, selectivity control in avoiding over hydrogenation of the imines or dehydrogenation of secondary amines remain as the big issues in practical applications [37]. Therefore, delicately designed catalysts and careful control of the reaction conditions (i.e., solvent, additional base, and temperature) are always required in general [23,29–32]. This calls for an alternative environmentally friendly process to decouple the synthesis of imines and secondary amines.

Intuitively, the synthesis of imine via cross-coupling of aniline and alcohol is a stepwise dehydrogenation-condensation process, whereas for secondary amine, the overall reaction can be simplified as a direct dehydrative coupling process (bottom of Scheme 1). In the presence of suitable catalysts, this strategy separates the synthesis of imine and secondary amine, thus avoiding the disadvantages in the conventional pathways. Since aniline is involved in the reaction from the second step, manipulating the activation of alcohol is the key in realizing this strategy. That is, while the oxidation of the alcohol into aldehyde and H atoms leads to the formation of imine, the mild activation of alcohol might be able to facilitate the direct dehydrative coupling. To the best of our knowledge, this strategy has not yet been attempted in practical synthesis.

Surface engineering of a photocatalyst is frequently explored in generating tuneable oxidative species [38–40], thus offering a platform for controlled oxidation of reactants. In particular, the presence of a metal cocatalyst significantly may influence the sorption and activation pathways of surface adsorbed species (i.e., hydrogen atoms, amines,

benzyl radicals) and eventually the final products [41,42]. It has been reported that the presence of Pd cocatalysts with suitable sizes promote the photocatalytic hydrogenation of imine into secondary amine owing to a preferential adsorption of imine over alcohol [43]. However, the synthesis of secondary amine still proceeds via the conventional hydrogen borrowing pathway. Our previous investigations show that the presence of a noble metal cocatalyst (i.e., Pt, Pd, Au) is very efficient in abstracting hydrogen from alcohols for a series of reactions that involves a hydrogen atom transfer step [41]. It is also noticed that some metals are less or not active for dehydrogenation of alcohols (i.e., Ag, Cu, Co) [44], indicating that a controlled activation of alcohol for cross-coupling with aniline might be realized by modulating the identity of metal cocatalyst. Up to now, the proposed strategy for selective cross-coupling of aniline and alcohol has not been realized yet.

Here we have explored a series of transition metals as cocatalyst on TiO₂ to manipulate the photo-activation of aromatic alcohols to realize their selective cross-coupling with anilines under mild reaction conditions. While Rh promotes the formation of imines via a stepwise dehydrogenative-condensation process, Fe favors the synthesis of secondary amines through a mild and direct condensation pathway. The catalytic performance in terms of reaction rate, stability, and substrate scope, as well as reaction pathways, intermediates, and active sites are investigated.

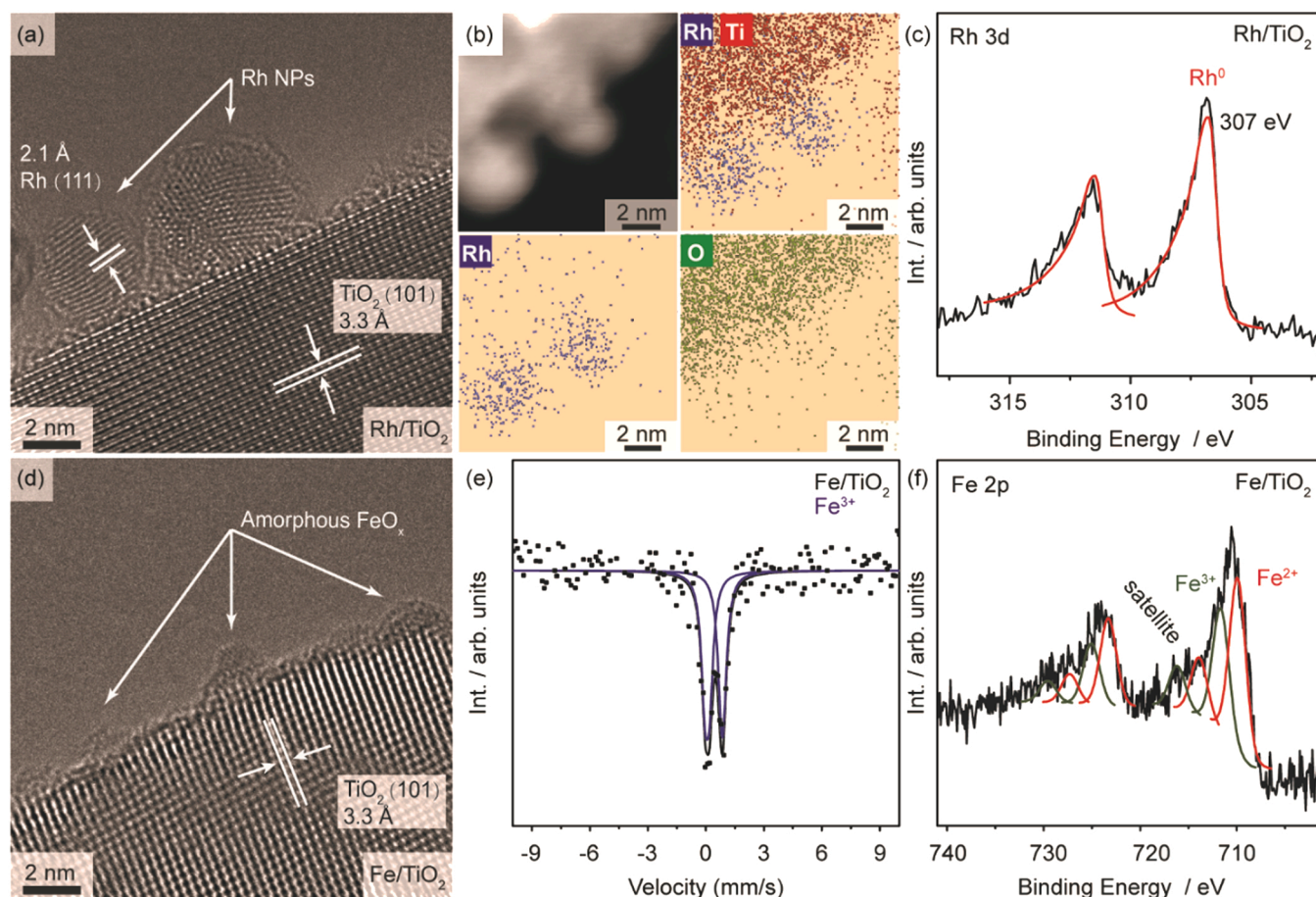


Fig. 1. Characterization of the as-synthesized photocatalysts. (a)–(c) TEM image, mapping, and Rh3d XPS spectrum of Rh/TiO₂. (d)–(f) TEM image, Mössbauer and Fe2p XPS spectra of Fe/TiO₂.

2. Experimental section

2.1. Chemicals & synthesis of metal decorated TiO₂

All chemicals are analytical grade and were used without further purification. A photodeposition method is employed for the synthesis of metal decorated TiO₂ (Degussa Aeroxide@P25) [45,46] with an intended loading of 1 wt% for all metals. A series of metal salts, including RhCl₃·3H₂O, H₂PtCl₆, CuCl₂·2H₂O, Ni(NO₃)₂·6H₂O, RuCl₃·xH₂O, Co(NO₃)₂·6H₂O, Ir(NO₃)₃, HAuCl₄·4H₂O, PdCl₂, AgNO₃ and FeCl₃·6H₂O were used as precursors for the synthesis of metal/TiO₂ (M/TiO₂). The real loadings determined by inductively coupled plasma-atomic emission spectroscopy (ICP-AES) are shown in Table S1 of the Supporting Information.

2.2. Characterizations

Transmission electron microscopy (TEM, FEI TALOS F200A) was used to study the morphology of samples at an accelerating voltage of 200 kV. X-ray photoelectron spectroscopy (XPS, K-alpha, Thermo Fisher Scientific) was used to study the surface chemical composition of the samples. The instrument was equipped with a monochromatic Al Kα X-ray source. The ultraviolet photoelectron spectroscopy (UPS, TalosTM 200A) was performed in ultrahigh vacuum (< 10^{−10} Torr) using He I (21.2 eV) as the light source. The Mössbauer spectroscopy is performed using a MR-351 compact driving system with ⁵⁷Co as the radioactive source moving in a constant acceleration mode. The velocity of the instrument was corrected using an α-Fe foil (15 μm) as reference. Diffuse reflectance spectroscopy (DRS, UH4150, Hitachi) equipped with a

spherical integrating detector was used to analyze the optical properties of the photocatalysts. Photoluminescence spectra were measured using an FLS 1000 spectrometer (Edinburgh Instruments) that is equipped with a fast lifetime MCP detector. A 60 W xenon lamp was used as the light source.

2.3. Performance evaluation & mechanism analysis

The photocatalytic coupling reaction of benzyl alcohol and aniline was performed using reaction mixture consisting of 10 mg photocatalyst, 22 μmol of benzyl alcohol and 20 μmol aniline in 2 mL of n-hexane solution. The liquid phase products were analyzed by gas chromatography with mass spectrometry (GC-MS, Agilent GC 7890 GC system coupled with 5973 network mass selective detector) and nuclear magnetic resonance (NMR, Bruker AVANCE III 400 M).

The evolution of gas phase products was determined by a quadrupole mass spectrometer (MS, HPR-20, Hiden) equipped with an in-situ reactor. Adsorption and dissociation of benzyl alcohol on different catalysts were analyzed by post mortem temperature programmed desorption (P-TPD) using a chemisorption analyzer (AutoChem II) coupled with a MS (OmniStar GSD, Pfeiffer) and in-situ Fourier transform infrared (FTIR) spectrometer (VERTEX 70, Bruker). The radical species were analyzed by electron spin resonance spectrometer (ESR, JES FA-200, JEOL) using N-tert-butyl-α-phenylnitron (PBN) as the spin trap.

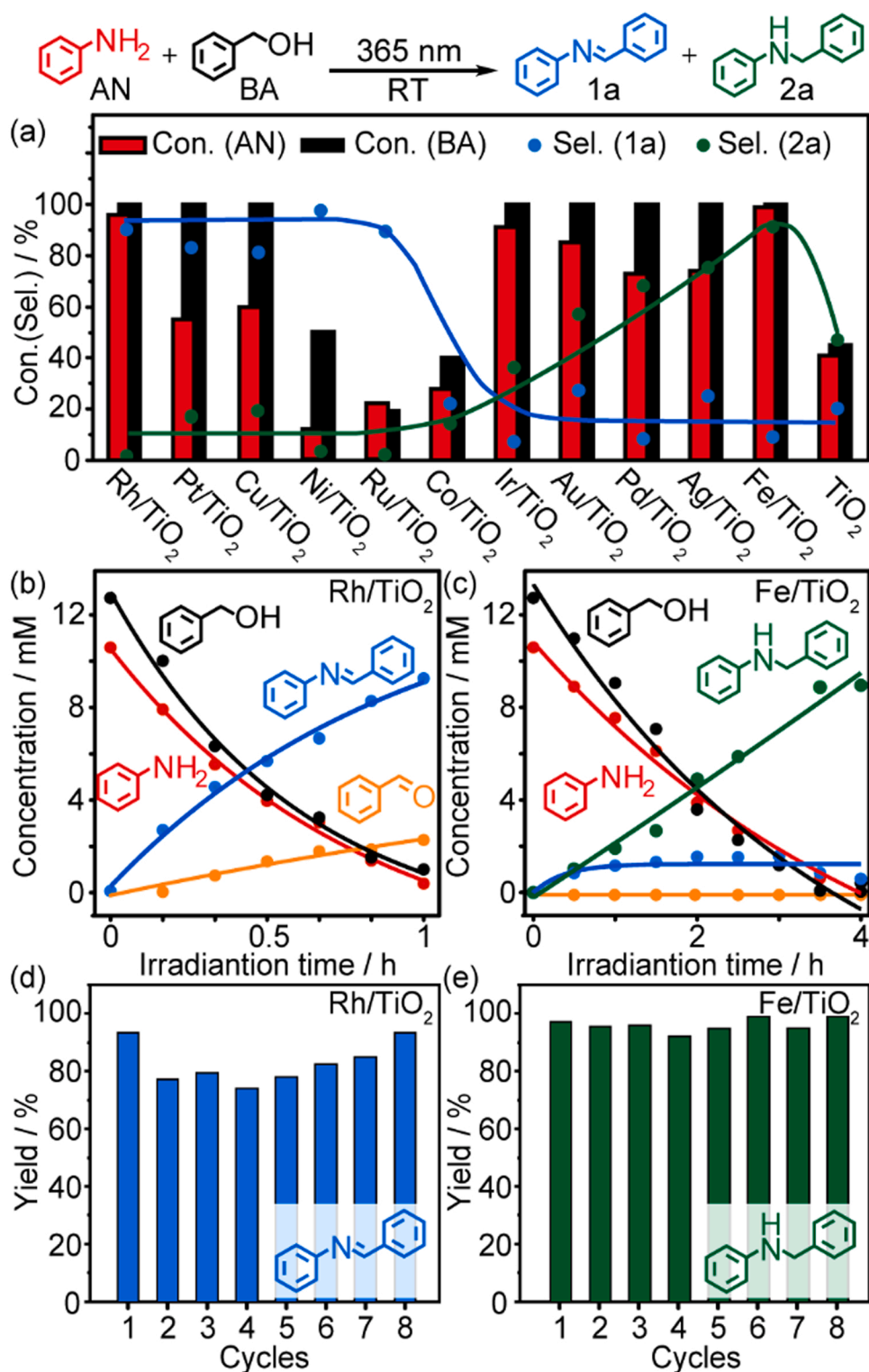


Fig. 2. Photocatalytic cross-coupling of aniline (AN) and benzyl alcohol (BA) using various metals supported on TiO₂. (a) The effect of metal identity for an irradiation time of 4 h. (b) and (c) Time-course of the photocatalytic process using Rh/TiO₂ and Fe/TiO₂. (d) and (e) Stability of Rh/TiO₂ and Fe/TiO₂ in cross-coupling of AN and BA. Reaction conditions: 10 mg catalyst, 10 mM AN and 12 mM BA in 2 mL n-hexane under 365 nm irradiation (LED, 14 mW·cm⁻²) at RT and 1 bar N₂ conditions. The irradiation time for Rh/TiO₂ and Fe/TiO₂ in stability tests are 1 h and 4 h, respectively.

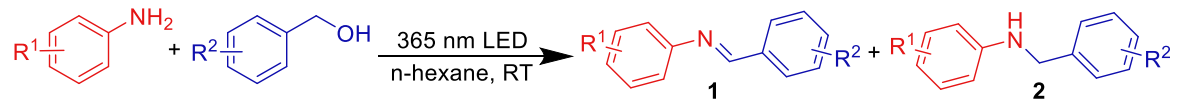
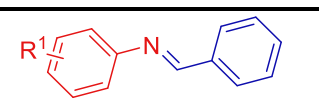
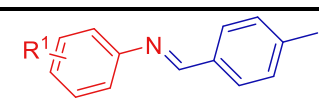
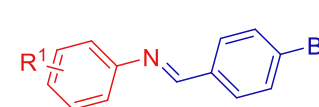
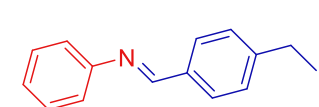
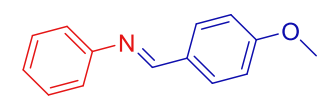
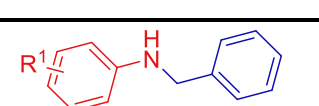
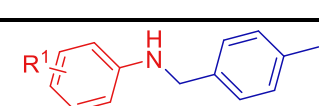
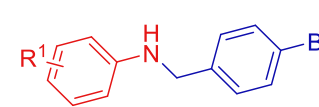
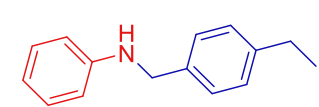
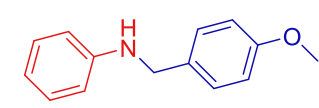
3. Results and discussion

3.1. Characterization of the photocatalysts

The Rh and Fe cocatalyst decorated TiO₂ photocatalysts (Rh/TiO₂ and Fe/TiO₂) are synthesized through a photodeposition method using RhCl₃·3H₂O and FeCl₃·6H₂O as precursors (Supporting Note 1) [45]. Though the loadings of Rh and Fe are different (0.9 and 0.2 wt% Supporting Table S1), it is less likely to influence the reaction mechanism

and selectivity. The single Rh nanoparticles (NPs) supported on TiO₂ present an interplanar spacing of 2.1 Å in high-angle annular dark field-scanning transmission electron microscopy (HAADF-STEM, Fig. 1a), which agrees well with the (111) lattice planes of metallic Rh. Elementary mapping reveals that the Rh NPs form an interface with the TiO₂ support (Fig. 1b). Oxygen is only observed within the TiO₂ domains, confirming the metallic state of Rh cocatalyst. The Rh NPs are homogeneously dispersed on TiO₂, as revealed by the microscopic imaging (Fig. S1a and S1b). The averaged particle size is 2.7 nm with both

Table 1Substrate scope of photocatalytic cross-coupling of anilines and alcohols using Rh/TiO₂ and Fe/TiO₂.^a

			
Rh/TiO₂			
			
R¹ = H	1a. Con. 96%; Sel. 90% ^b	R¹ = H	1f. Con. 85%; Sel. 99%
p-Me	1b. Con. 83%; Sel. 96%	p-Me	1g. Con. 78%; Sel. 99%
p-Et	1c. Con. 91%; Sel. 99%	p-Et	1h. Con. 71%; Sel. 99%
p-MeO	1d. Con. 85%; Sel. 99%	p-MeO	1i. Con. 92%; Sel. 99%
m-Cl	1e. Con. 73%; Sel. 99%	m-Cl	1j. Con. 60%; Sel. 99%
			
R¹ = H	1k. Con. 85%; Sel. 99%		1o. Con. 79%; Sel. 99%
p-Me	1l. Con. 77%; Sel. 99%		
p-Et	1m. Con. 73%; Sel. 99%		
m-Cl	1n. Con. 70%; Sel. 99%		
			1p. Con. 78%; Sel. 99%
Fe/TiO₂			
			
R¹ = H	2a. Con. 99%; Sel. 91% ^c	R¹ = H	2f. Con. 94%; Sel. 90%
p-Me	2b. Con. 95%; Sel. 79%	p-Me	2g. Con. 99%; Sel. 95%
p-Et	2c. Con. 97%; Sel. 89%	p-Et	2h. Con. 99%; Sel. 99%
p-MeO	2d. Con. 95%; Sel. 99%	p-MeO	2i. Con. 95%; Sel. 73%
m-Cl	2e. Con. 95%; Sel. 99%	m-Cl	2j. Con. 94%; Sel. 93%
			
R¹ = H	2k. Con. 95%; Sel. 85%		2o. Con. 88%; Sel. 84%
p-Me	2l. Con. 97%; Sel. 85%		
p-Et	2m. Con. 95%; Sel. 80%		
m-Cl	2n. Con. 54%; Sel. 87%		
			2p. Con. 93%; Sel. 78%

[a] Reaction conditions: 10 mg catalyst, 10 mM aniline and 12 mM alcohol in 2 mL n-hexane solution under 1 bar N₂ atmosphere, 365 nm LED irradiation for 24 h (14 mW·cm⁻²). [b] Same as a, 1 h irradiation; [c] Same as a, 4 h irradiation. Con.: conversion, Sel.: selectivity.

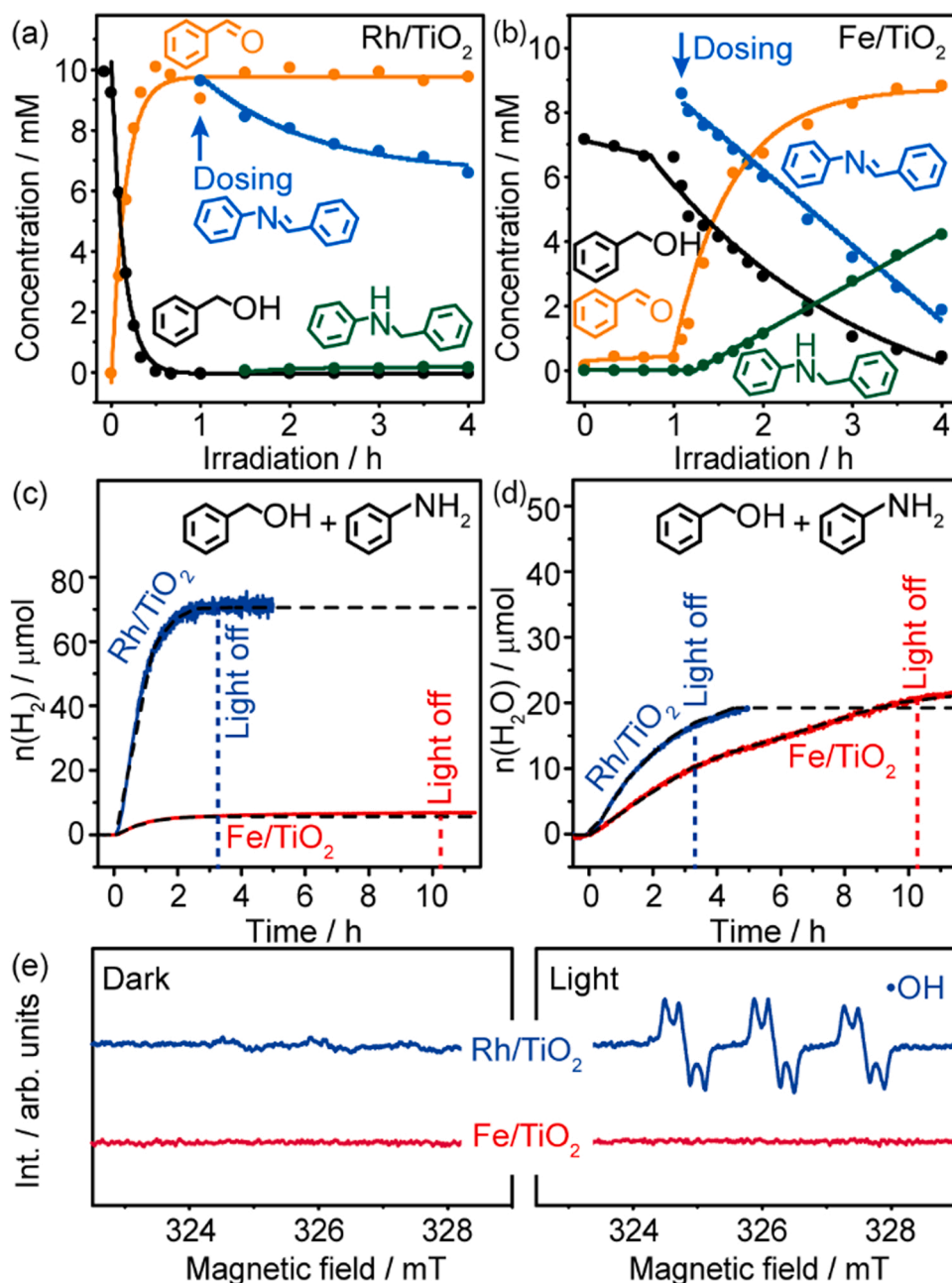


Fig. 3. Reaction mechanisms. (a) and (b) Stepwise photocatalytic conversion of benzyl alcohol and imine using Rh/TiO₂ and Fe/TiO₂. Reaction conditions: 100 mg catalyst in 20 mL n-hexane under 1 bar N₂ atmosphere, 365 nm LED irradiation (14 mW·cm⁻²). (c) and (d) Evolution of H₂ and water vapor during photocatalytic cross-coupling of aniline and benzyl alcohol on Rh/TiO₂ and Fe/TiO₂. Reaction conditions: 30 mg catalyst with 100 μmol aniline and benzyl alcohol under 1 bar Ar atmosphere, 365 nm LED irradiation (14 mW·cm⁻²). (e) ESR spectra of Rh/TiO₂ and Fe/TiO₂ suspensions in DMSO under dark and irradiation conditions using PBN as the spin trap.

small Rh NPs (~1 nm) and slightly larger NPs (~5 nm) observed (Fig. S1c). The survey scan of XPS reveals that the Rh/TiO₂ is chemically clean (Fig. S1d). The Rh NPs are predominantly metallic (Rh3d = 307 eV) according to the region of interest XPS (Fig. 1c).

In comparison, no metallic Fe NPs are observed on the as-synthesized Fe/TiO₂ (Fig. 1d and Fig. S2). The lattice fringes with interplanar spacing of 3.4 Å are indexed to the (101) crystal plane of anatase TiO₂. Instead, some amorphous species are observed on TiO₂, which are probably iron oxides, as the photogenerated electron on TiO₂ is inefficient in reducing Fe³⁺ into metallic Fe due to the redox potential. Interestingly, Fe metal NPs with an average size of ~3.1 nm evolve on TiO₂ homogeneously during TEM analysis (Fig. S2a-f). This beam induced reduction of Fe confirms the TiO₂ surface is originally covered with amorphous iron oxides. The presence of iron oxides is further confirmed by the Mössbauer spectrum (Fig. 1e), which is characteristic for well dispersed Fe(III) oxide, as observed before on TiO₂ [47]. This agrees with the XPS analysis of Fe2p (Fig. 1f), where Fe²⁺ and Fe³⁺ are

observed on the surface of TiO₂ (Fig. 1f). The oxidation states of Ti2p and O1s in Fe/TiO₂ remain unchanged in comparison with pristine TiO₂ (Fig. S3), indicating that the iron oxide species are dispersed on TiO₂ rather than doped into the lattice.

The band gaps (E_g) of Rh/TiO₂ and Fe/TiO₂ are 3.0 eV, which are slightly reduced compared to that of the pristine TiO₂ according to DRS (Fig. S4a). UPS reveals that the slightly reduced E_g is due to the shift of both the valence band (VB, 0.1 eV) and the conduction band (CB, 0.3 eV), respectively (Fig. S4b and S4c). In addition, a significant reduction of the emission intensity is observed for both Rh/TiO₂ and Fe/TiO₂ in photoluminescence spectroscopy (PL), suggesting that the presence of Rh and Fe prolong the lifetime of the photogenerated charge carriers, thus benefiting the photocatalytic performances (Fig. S4d).

3.2. Catalytic performance

We have first evaluated a series of metal cocatalysts supported on

TiO₂ for photocatalytic cross-coupling of aromatic amine and alcohol employing aniline (AN, 10 mM) and benzyl alcohol (BA, 12 mM) as the model compounds under 365 nm irradiation at room temperature (RT) and deaerated conditions (Fig. 2a). Rh modified TiO₂ fully converts AN and BA simultaneously into the corresponding imine (N-benzylideneaniline, **1a**) with excellent selectivity via the ADC path. While Pt and Cu show high selectivity towards **1a**, poor conversion of AN results in a reduced production of **1a** and increased generation of unwanted benzaldehyde as byproduct. Ni, Ru, and Co are also not promising as they are inactive for the conversion of both AN and BA. The selectivity towards the secondary amine (N-benzylaniline, **2a**) gradually increases in the order of Ir < Au < Pd < Ag < Fe. The Fe/TiO₂ photocatalyst outperforms other candidates owing to a full conversion of both AN and BA. In comparison, both the pristine TiO₂ and a photodeposition treated pristine TiO₂ (metal precursor free) present poor conversion and selectivity in the cross-coupling of AN and BA, confirming the essential role of the metal cocatalyst (Fig. S5). No reaction occurs in the absence of either irradiation or a photocatalyst.

The time dependence of photocatalytic cross-coupling of anilines and alcohols using Rh/TiO₂ and Fe/TiO₂ has been investigated under identical conditions (Figs. 2b and 2c). Upon irradiation, AN and BA are completely consumed within 1 h for Rh/TiO₂ and display a first-order kinetics with a similar rate constant of 1.44 h⁻¹, suggesting a 1:1 stoichiometric reaction of both reactants (Fig. 2b). While the evolution of **1a** follows an exponential trend, a small quantity of benzaldehyde forms with almost zero-order kinetics. Since the zero-order reaction is an indication of rate determining step (RDS), it implies that benzaldehyde is the key intermediate during the formation of **1a** when Rh/TiO₂ is used. Photogenerated **1a** cannot be further hydrogenated into **2a** with prolonged irradiation times up to 4 h, as the molecular hydrogen escapes into the gas phase (Fig. S6a). In comparison, the consumption of AN and BA also displays a similar first-order kinetics for Fe/TiO₂, though a smaller rate constant (0.24 h⁻¹) is noted (Fig. 2c). Here **2a** is the major product within the 4 h irradiation course with only trace amounts of **1a** (~1 mM). The formation of **2a** exhibits a zero-order kinetics without evolution of benzaldehyde, suggesting that AN and BA are directly coupled into **2a** rather than via the ADC process. Besides, the concentration of alcohol is almost in stoichiometric with aniline (1.2:1), which rules out the formation of secondary amine via the ADC-BH pathway using Fe/TiO₂, as molecular hydrogen will be released and lost during the formation of imine. Additionally, we have also investigated Pt/TiO₂ and Pd/TiO₂ as representative photocatalysts with slightly reduced selectivity to **1a** and **2a**, respectively (Fig. S6b and 6c). In both cases, the relatively low selectivity to desired product is mainly due to the incomplete consumption of aniline. Both Rh/TiO₂ and Fe/TiO₂ exhibit a high stability for the selective synthesis of **1a** and **2a** via cross-coupling of AN and BA (Figs. 2d and 2e). Stable yields of ~80% for **1a** and ~95% for **2a** over Rh/TiO₂ and Fe/TiO₂ are maintained within eight cycles, which looks promising for applications.

3.3. Substrate scope

Table 1 summarizes the general applicability of the Rh/TiO₂ and Fe/TiO₂ photocatalysts in photocatalytic cross-coupling of a series of aromatic aniline and alcohol substrates (Fig. S7-S45). Aromatic anilines with electron donating groups (EDG) show excellent conversions and selectivities for the synthesis corresponding imines with benzyl alcohol using Rh/TiO₂ as the photocatalyst (Tables 1, 1a-1d). The m-chloro-benzyl aniline displays a slightly reduced conversion (Tables 1, 1e), possibly due to the presence of an electron withdrawing group (EWG). The presence of EDG (p-methyl, p-ethyl, and p-methoxy) or EWG (p-bromo) on the aromatic alcohol does not significantly influence conversion and selectivity (Tables 1, 1f-1i, 1k-1m, 1o and 1p) except, however, when halide functionalized aniline is used as substrate, which leads to slightly decreased conversion (1j and 1n). The synthesis of secondary amine using Fe/TiO₂ shows excellent tolerance of EDG and

EWG on either aniline and alcohol with high conversions and selectivities in most cases (**2a-2m**, **2o**, and **2p**). The only exception is the cross-coupling of m-chloro-benzyl aniline with p-bromo-benzyl alcohol (**2n**), possibly due to the EWGs on both reactants that apparently deactivate the reaction.

3.4. Reaction mechanisms

We expect that Rh/TiO₂ facilitates the cross-coupling of aniline and alcohol via the ADC path for the formation of imines owing to the high performance of Rh in alcohol dehydrogenation [48,49], whereas Fe/TiO₂ promotes the synthesis of secondary amine via a direct condensation due to the weak activation of the alcohol. This is first verified by step-wise photocatalytic conversion of benzyl alcohol and imine (Figs. 3a and b). When only benzyl alcohol is added into the reaction system, the formation of benzaldehyde finishes within 1 h of irradiation on Rh/TiO₂. The concentration of benzaldehyde remains unchanged when **1a** is added thereafter, implying that the abstracted hydrogen atoms desorb as H₂ and thus cannot be used for hydrogenation of **1a**. The decline of **1a** is due to the polymerization of imine into tertiary amine according to GC-MS analysis (Fig. S46a-c) [14]. Note that **2a** cannot be generated even by adding **1a** prior to the complete conversion of benzyl alcohol into benzaldehyde, suggesting that Rh/TiO₂ cannot hydrogenate imine using molecular hydrogen. (Fig. S46c). In comparison, no benzaldehyde is formed upon irradiation using Fe/TiO₂ with benzyl alcohol as the sole reactant (Fig. 3b), though a slight decrease of the benzyl alcohol occurs. This may associate to the adsorption and mild activation of benzyl alcohol on Fe/TiO₂ and will be discussed afterwards. Interestingly, a linear conversion of **1a** into **2a** accompanied with an exponential conversion of benzyl alcohol into benzaldehyde is observed upon addition of **1a** into the system under irradiation. This indicates that Fe/TiO₂ is capable of extracting hydrogen from the alcohol and donating it to the imine, where the hydrogenation of imine is the RDS. Therefore, when benzyl alcohol is replaced by benzaldehyde to react with aniline using Fe/TiO₂, only **1a** can be produced via the condensation process due to the lack of hydrogen atom (Fig. S46d). In addition, no reaction is observed when aniline is the sole reactant for both Rh/TiO₂ and Fe/TiO₂ (Fig. S47), confirming that activation of alcohol is the first step in cross-coupling for both photocatalysts.

We have further analyzed the evolution of gas-phase products during photocatalytic cross-coupling of aniline and benzyl alcohol by in-situ mass spectrometry (MS) to examine the catalytic role of Rh and Fe (Figs. 3c and 3d). Prior to the analysis, Ar purging is employed to remove O₂ down to ~100 ppm (Fig. S48). As expected, a rapid evolution of molecular hydrogen is observed for Rh/TiO₂ under irradiation in the presence of aniline and benzyl alcohol, confirming that Rh/TiO₂ favors the formation of **1a** due to the rapid releasing of H₂ (Fig. 3c). The quantity of photogenerated H₂ reaches a plateau at ~70 μmol at prolonged irradiation time due to the full conversion of benzyl alcohol (~100 μmol), and the absence of a decrease of H₂ suggests that Rh/TiO₂ do not further hydrogenate **1a** to **2a**. The slight mismatch between experimental and ideal quantities of photogenerated H₂ relates to the loss of benzyl alcohol during Ar purging prior to irradiation. In comparison, only a negligible amount of H₂ is detected for Fe/TiO₂. This might be associated with the adsorption of hydrogen atoms, which is stronger on Fe (-0.50 eV) [50] than on Rh (-0.32 eV) [51], or alternatively, because photocatalytic cross-coupling of aniline with alcohol on Fe/TiO₂ does not proceed via the generation of photogenerated hydrogen atoms. Meanwhile, the increase of water vapor is also observed for both photocatalysts upon irradiation. Though Rh/TiO₂ presents a faster kinetics in the evolution of water than Fe/TiO₂ due to faster formation of **1a** than **2a** (Figs. 2b and 2c), the overall quantity of water vapor in gas-phase is almost identical for both cases (20 μmol). This suggests that aniline and benzyl alcohol are fully consumed in both cases for cross-coupling in both cases. In addition, no evolution of H₂ and H₂O is observed when pristine TiO₂ is used (Fig. S48).

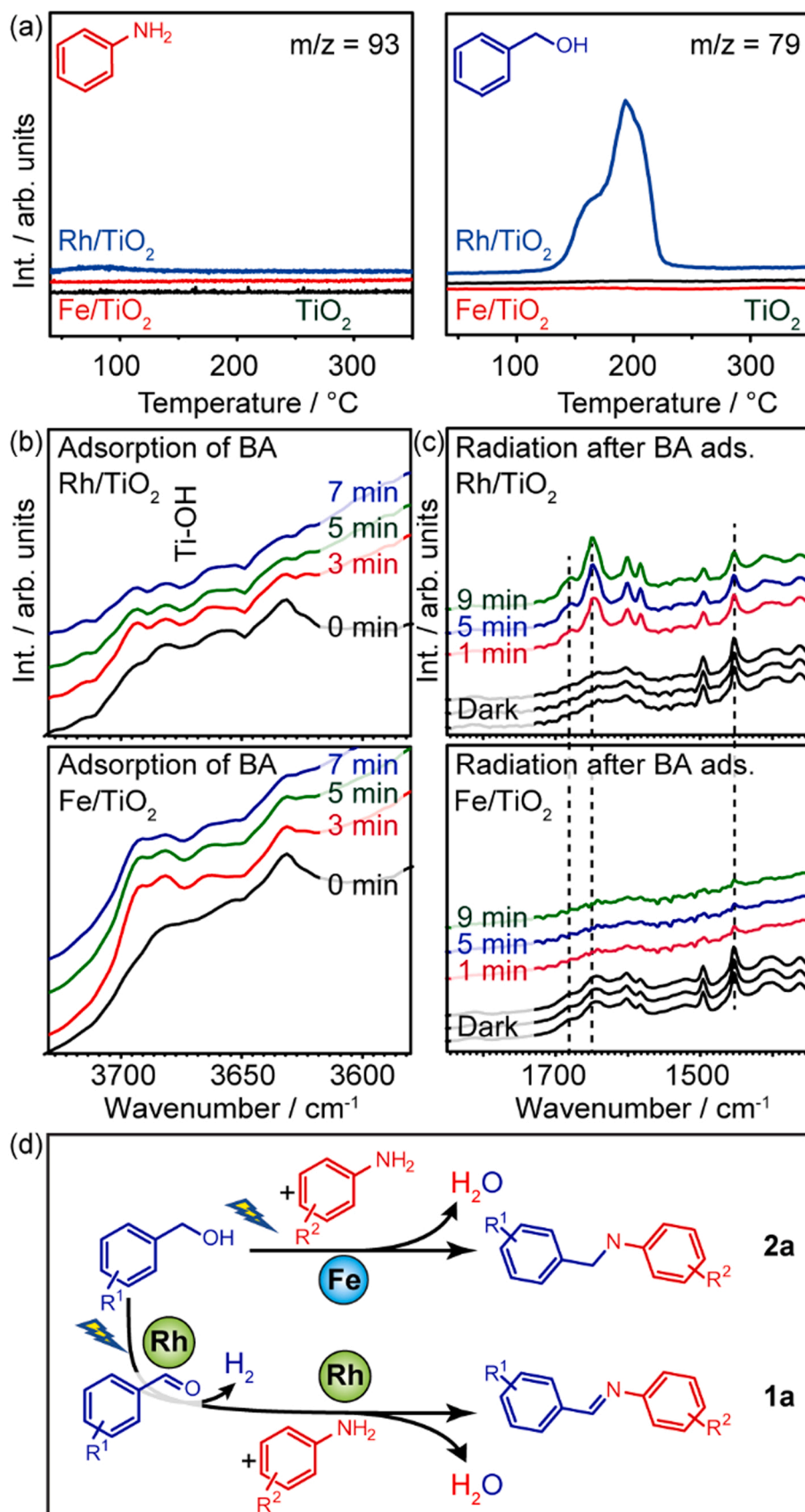


Fig. 4. Reaction mechanisms. (a) TPD analysis of aniline and benzyl alcohol adsorption on TiO_2 , Rh/TiO_2 and Fe/TiO_2 , respectively. (b) and (c) DRIFT analysis of benzyl alcohol (BA) adsorption and conversion upon irradiation on Rh/TiO_2 and Fe/TiO_2 . (d) Proposed reaction pathways for metal mediated photocatalytic cross coupling of aniline and aromatic alcohol.

A previous report on Pd modified TiO₂ photocatalyst suggests that imine is the intermediate in the synthesis of secondary amine via cross-coupling of aniline and alcohol (alcohol as solvent) [43]. In this case, the excessive alcohol is a reservoir that provide sufficient hydrogen to hydrogenate the imines. However, this is less unlikely in our case, as benzyl alcohol is present in stoichiometric amount with aniline, thus is insufficient to afford extra hydrogen once released as H₂. Also, neither benzaldehyde nor imine are observed in the time-course for Fe/TiO₂ (Fig. 2c). This is confirmed by the ESR analysis of Rh/TiO₂ and Fe/TiO₂ in dimethyl sulfoxide (DMSO) with PBN as the spin-trap (Fig. 3e). While both Rh/TiO₂ and Fe/TiO₂ are almost silent under dark conditions, the formation of •OH radicals are observed for Rh/TiO₂ after irradiation. In contrast, the Fe/TiO₂ shows a very weak signal of •OH radical under irradiation. This indicates that Fe/TiO₂ displays a slow oxidation kinetics in dissociation of the O-H bond in benzyl alcohol under irradiation to abstract hydrogen and generate aldehyde, but rather activate the alcohol mildly for direct condensation with aniline.

The adsorption of the reactants is further studied to probe the role of Rh and Fe cocatalysts in cross-coupling of aniline and alcohol. Both TiO₂, Rh/TiO₂ and Fe/TiO₂ show poor adsorption of aniline ($m/z = 93$) in terms of quantity and strength according to the P-TPD spectra of pre-adsorbed aniline (Fig. 4a). In comparison, an intense desorption peak of benzyl alcohol ($m/z = 79$) is observed for Rh/TiO₂ at 192 °C, whereas the TiO₂ and Fe/TiO₂ show no detectable desorption peak. The presence of Rh favors mild adsorption of benzyl alcohol at moderate temperature, which is beneficial for photocatalytic dehydrogenation of benzyl alcohol, thus accelerating the coupling reaction rate to yield **1a**.

We have further employed diffuse reflectance infrared Fourier transform spectroscopy (DRIFT) to investigate the adsorption sites of benzyl alcohol on the photocatalysts. Prior to dosing of benzyl alcohol, both Rh/TiO₂ and Fe/TiO₂ present a characteristic vibrational peak at $\sim 3677\text{ cm}^{-1}$ that can be assigned to Ti-OH [52]. This peak is absent for Rh/TiO₂ after reaching an equilibrium of the ad/desorption of dosed benzyl alcohol (Fig. 4b, top), suggesting that benzyl alcohol adsorbs on the surface hydroxyl of Rh/TiO₂, possibly via the formation of a hydrogen bond. In contrast, the Ti-OH peak remains as is for Fe/TiO₂ after dosing benzyl alcohol, indicating a poor interaction between the photocatalyst and the reactant that matches well with the TPD analysis. Interestingly, Rh/TiO₂ and Fe/TiO₂ display opposite features upon irradiation with the presence of benzyl alcohol. The evolution of carbonyl (stretch vibration of C=O, 1680 cm^{-1}) and water (bending vibration of O-H, 1650 cm^{-1}) is only observed for Rh/TiO₂, suggesting the oxidation of benzyl alcohol into benzaldehyde and water on Rh/TiO₂ (Fig. 4c, top). It is worthy to note that while the bending of O-H of benzyl alcohol ($\sim 1455\text{ cm}^{-1}$) is only slightly decreased on Rh/TiO₂, such feature completely disappeared on Fe/TiO₂ (Fig. 4c, bottom). This confirms that the presence of Fe does not convert benzyl alcohol into benzaldehyde and H₂, but leads to a transition state that directly couples with aniline when present. Based on these results, we propose a reaction mechanism of Rh and Fe mediated photocatalytic cross coupling of aniline and aromatic alcohol (Fig. 4d). When Rh is employed as the cocatalyst, the strong adsorption of alcohol and its high dehydrogenation power result in rapid photo-conversion of aromatic alcohol into corresponding aldehyde with liberation of molecular hydrogen, thus facilitating the condensation coupling of photogenerated aldehyde with aniline to yield imines. In the case of Fe cocatalyst, the aromatic alcohol molecule is weakly adsorbed on the photocatalyst and is only mildly activated without the formation of aldehyde and molecular hydrogen under irradiation, thus allowing a direct dehydrative coupling with aniline to produce secondary amines.

4. Conclusion

Herein, we present a tunable photocatalytic process mediated by metal cocatalyst for the synthesis of imines and secondary amines via cross-coupling of aromatic aniline and alcohol. While Rh cocatalyst

supported on TiO₂ facilitates the synthesis of imine via the conventional stepwise dehydrogenative-condensation pathway, the Fe cocatalyst promotes the production of secondary amine via a direct condensation approach. Mechanistic analysis reveals that the identity of metal species mediates adsorption and activation of alcohols, thus manipulating the reaction pathways. Rh exhibits strong adsorption of alcohol with high dehydrogenation power, thus leading to a rapid condensation of photogenerated aldehyde with aniline. In contrast, alcohol molecules weakly adsorb on Fe and are only mildly activated without the formation of aldehyde under irradiation, thus allowing a direct dehydrative coupling with aniline. Both Rh/TiO₂ and Fe/TiO₂ photocatalysts show high stability and a wide substrate scope, featuring such process promising for applications.

CRediT authorship contribution statement

Dongdong Lv, Yaru Li & Wei Qiao: Investigation; Formal analysis; Visualization; Writing - Review & Editing. **Dongdong Zhang, Yuan-qiang Mai & Nengjun Cai:** Investigation; Formal analysis. **Hongwei Xiang & Yongwang Li:** Resources. **J. W. (Hans) Niemantsverdriet & Weichang Hao:** Resources; Writing - Review & Editing. **Ren Su:** Conceptualization; Methodology; Validation; Resources; Writing - Original Draft; Writing - Review & Editing; Supervision; Funding acquisition.

Declaration of Competing Interest

The authors declare that they have no known competing financial interests or personal relationships that could have appeared to influence the work reported in this paper.

Acknowledgments

RS and WH thank the National Natural Science Foundation of China (NSFC) for financial support (Project Nos. 21972100, 52073006, 11874003, 51672018). RS acknowledges the Priority Academic Program Development of Jiangsu Higher Education Institutions (PAPD, project No.: NH10800120) and WH acknowledges Beijing Natural Science Foundation (Z180007) and National Key R&D Program of China (2018YFE0202700).

Authors contributions

DL, YL, and WQ contribute equally to the work. RS conceived the studies. YL and DL synthesized the catalysts. DL performed the photocatalytic tests and YL explored the mechanism. DL, YL, DZ and WQ carried out the material characterizations. HX, YL, HN, WH and RS were involved in the design of the experiments, the discussion of the results, and the writing of the manuscript.

Appendix A. Supporting information

Supplementary data associated with this article can be found in the online version at [doi:10.1016/j.apcatb.2022.121264](https://doi.org/10.1016/j.apcatb.2022.121264).

References

- [1] O.I. Afanasyev, E. Kuchuk, D.L. Usanov, D. Chusov, Reductive amination in the synthesis of pharmaceuticals, *Chem. Rev.* 119 (2019) 11857–11911.
- [2] S. Bähn, S. Imm, L. Neubert, M. Zhang, H. Neumann, M. Beller, The catalytic amination of alcohols, *ChemCatChem* 3 (2011) 1853–1864.
- [3] K.S. Hayes, Industrial processes for manufacturing amines, *Appl. Catal. A* 221 (2001) 187–195.
- [4] E. Creutz Sidney, J. Lotito Kenneth, C. Fu Gregory, C. Peters Jonas, Photoinduced ullmann C–N coupling: demonstrating the viability of a radical pathway, *Science* 338 (2012) 647–651.

- [5] S. Biswas, B. Dutta, K. Mullick, C.-H. Kuo, A.S. Poyraz, S.L. Suib, Aerobic oxidation of amines to imines by cesium-promoted mesoporous manganese oxide, *ACS Catal.* 5 (2015) 4394–4403.
- [6] B. Górski, A.-L. Barthelemy, J.J. Douglas, F. Juliá, D. Leonori, Copper-catalysed amination of alkyl iodides enabled by halogen-atom transfer, *Nat. Catal.* 4 (2021) 623–630.
- [7] A.M. Wilders, J. Henle, M.C. Haibach, R. Swiatowicz, J. Bien, R.F. Henry, S. O. Asare, A.L. Wall, S. Shekhar, Pd-catalyzed cross-coupling of hindered, electron-deficient anilines with bulky (hetero)aryl halides using biaryl phosphorane ligands, *ACS Catal.* 10 (2020) 15008–15018.
- [8] R.C. Chikate, D.R. Petkar, B.S. Kadu, A.P. Jakhade, Fe–Ni/MMT nanocomposites as efficient H₂ generation catalyst: tandem approach towards one-pot synthesis of secondary amines, *Int. J. Hydrog. Energy* 45 (2020) 31798–31811.
- [9] B. Wang, Z. Deng, X. Fu, C. Xu, Z. Li, Photodeposition of Pd nanoparticles on ZnIn₂S₄ for efficient alkylation of amines and ketones' α -H with alcohols under visible light, *Appl. Catal. B* 237 (2018) 970–975.
- [10] K.-i Shimizu, N. Imaiida, K. Kon, S.M.A. Hakim Siddiki, A. Satsuma, Heterogeneous Ni catalysts for N-alkylation of amines with alcohols, *ACS Catal.* 3 (2013) 998–1005.
- [11] A. Monopoli, P. Cotugno, M. Cortese, C.D. Calvano, F. Ciminale, A. Nacci, Selective N-alkylation of arylamines with alkyl chloride in ionic liquids: scope and applications, *Eur. J. Org. Chem.* 2012 (2012) 3105–3111.
- [12] D. Maiti, B.P. Fors, J.L. Henderson, Y. Nakamura, S.L. Buchwald, Palladium-catalyzed coupling of functionalized primary and secondary amines with aryl and heteroaryl halides: two ligands suffice in most cases, *Chem. Sci.* 2 (2011) 57–68.
- [13] K. Okano, H. Tokuyama, T. Fukuyama, Synthesis of secondary arylamines through copper-mediated intermolecular aryl amination, *Org. Lett.* 5 (2003) 4987–4990.
- [14] R.N. Salvatore, C.H. Yoon, K.W. Jung, Synthesis of secondary amines, *Tetrahedron* 57 (2001) 7785–7811.
- [15] M.V. Jiménez, J. Fernández-Tornos, M. González-Lainez, B. Sánchez-Page, F. J. Modrego, L.A. Oro, J.J. Pérez-Torrente, Mechanistic studies on the N-alkylation of amines with alcohols catalysed by iridium(i) complexes with functionalised N-heterocyclic carbene ligands, *Catal. Sci. Technol.* 8 (2018) 2381–2393.
- [16] M.Kainz Quirin, D.Matier Carson, A. Bartoszewicz, L.Zultanski Susan, C. Peters Jonas, C.Fu Gregory, Asymmetric copper-catalyzed C–N cross-couplings induced by visible light, *Science* 351 (2016) 681–684.
- [17] J.-C. Castillo, J. Orrego-Hernández, J. Portilla, Cs₂CO₃-promoted direct N-alkylation: highly chemoselective synthesis of N-alkylated benzylamines and anilines, *Eur. J. Org. Chem.* 2016 (2016) 3824–3835.
- [18] S. Rösler, M. Ertl, T. Irrgang, R. Kempe, Cobalt-catalyzed alkylation of aromatic amines by alcohols, *Angew. Chem. Int. Ed.* 54 (2015) 15046–15050.
- [19] K. Shimizu, M. Nishimura, A. Satsuma, γ -Alumina-supported silver cluster for N-benzoylation of anilines with alcohols, *ChemCatChem* 1 (2009) 497–503.
- [20] M.A. Ashley, T. Rovis, Photoredox-catalyzed deaminative alkylation via C–N bond activation of primary amines, *J. Am. Chem. Soc.* 142 (2020) 18310–18316.
- [21] X. Ye, P.N. Plessow, M.K. Brinks, M. Schelwies, T. Schaub, F. Rominger, R. Paciello, M. Limbach, P. Hofmann, Alcohol amination with ammonia catalyzed by an acridine-based ruthenium pincer complex: a mechanistic study, *J. Am. Chem. Soc.* 136 (2014) 5923–5929.
- [22] Y. Kita, M. Kuwabara, S. Yamadera, K. Kamata, M. Hara, Effects of ruthenium hydride species on primary amine synthesis by direct amination of alcohols over a heterogeneous Ru catalyst, *Chem. Sci.* 11 (2020) 9884–9890.
- [23] K. Paudel, S. Xu, O. Hietsoi, B. Pandey, C. Onuh, K. Ding, Switchable imine and amine synthesis catalyzed by a well-defined cobalt complex, *Organometallics* 40 (2021) 418–426.
- [24] A. Corma, T. Ródenas, M.J. Sabater, A. Bifunctional, Pd/MgO solid catalyst for the one-pot selective N-monoalkylation of amines with alcohols, *Chem. Eur. J.* 16 (2010) 254–260.
- [25] B. Chen, L. Wang, S. Gao, Recent advances in aerobic oxidation of alcohols and amines to imines, *ACS Catal.* 5 (2015) 5851–5876.
- [26] R. Deshidi, M.A. Rizvi, B.A. Shah, Highly efficient dehydrogenative cross-coupling of aldehydes with amines and alcohols, *RSC Adv.* 5 (2015) 90521–90524.
- [27] X. Huang, L. Liu, H. Gao, W. Dong, M. Yang, G. Wang, Hierarchically nanostructured MnCo₂O₄ as active catalysts for the synthesis of N-benzylideneaniline from benzyl alcohol and aniline, *Green Chem.* 19 (2017) 769–777.
- [28] S. Wu, W. Sun, J. Chen, J. Zhao, Q. Cao, W. Fang, Q. Zhao, Efficient imine synthesis from oxidative coupling of alcohols and amines under air atmosphere catalyzed by Zn-doped Al₂O₃ supported Au nanoparticles, *J. Catal.* 377 (2019) 110–121.
- [29] S. Rojas-Buzo, P. Concepción, A. Corma, M. Moliner, M. Boronat, In-Situ-Generated Active Hf-hydride in Zeolites for the Tandem N-Alkylation of Amines with Benzyl Alcohol, *ACS Catal.* 11 (2021) 8049–8061.
- [30] V. Goyal, N. Sarki, M.K. Poddar, A. Narani, D. Tripathi, A. Ray, K. Natte, Biorenewable carbon-supported Ru catalyst for N-alkylation of amines with alcohols and selective hydrogenation of nitroarenes, *N. J. Chem.* 45 (2021) 14687–14694.
- [31] M. Bagheri, M.Y. Masoomi, E. Domínguez, H. García, Cobalt-based quasi-metal-organic framework as a tandem catalyst for room-temperature open-air one-pot synthesis of imines, *ACS Sustain. Chem. Eng.* 9 (2021) 10611–10619.
- [32] W.S. Putro, T. Hara, N. Ichikuni, S. Shimazu, One-pot synthesis of aniline N-alkylation from benzyl alcohol over Cu-Fe catalyst, *Appl. Catal. A* 602 (2020), 117519.
- [33] R. Pothikumar, V.T. Bhat, K. Namitharan, Pyridine mediated transition-metal-free direct alkylation of anilines using alcohols via borrowing hydrogen conditions, *Chem. Commun.* 56 (2020) 13607–13610.
- [34] Y. Gong, Y. Yuan, C. Chen, S. Chaemchuen, F. Verpoort, Palladium metallated shell layer of shell@core MOFs as an example of an efficient catalyst design strategy for effective olefin hydrogenation reaction, *J. Catal.* 392 (2020) 141–149.
- [35] T. Tong, W. Guo, X. Liu, Y. Guo, C.-W. Pao, J.-L. Chen, Y. Hu, Y. Wang, Dual functions of CoOx decoration in PtCo/CeO₂ catalysts for the hydrogen-borrowing amination of alcohols to primary amines, *J. Catal.* 378 (2019) 392–401.
- [36] H. Xu, J.-L. Shi, H. Hao, X. Li, X. Lang, Visible light photocatalytic aerobic oxidative synthesis of imines from alcohols and amines on dye-sensitized TiO₂, *Catal. Today* 335 (2019) 128–135.
- [37] T. Wang, J. Ibañez, K. Wang, L. Fang, M. Sabbe, C. Michel, S. Paul, M. Pera-Titus, P. Sautet, Rational design of selective metal catalysts for alcohol amination with ammonia, *Nat. Catal.* 2 (2019) 773–779.
- [38] R. Su, R. Tiruvalam, A.J. Logsdail, Q. He, C.A. Downing, M.T. Jensen, N. Dimitratos, L. Kesavan, P.P. Wells, R. Bechstein, H.H. Jensen, S. Wendt, C.R. A. Catlow, C.J. Kiely, G.J. Hutchings, F. Besenbacher, Designer titania-supported Au–Pd nanoparticles for efficient photocatalytic hydrogen production, *ACS Nano* 8 (2014) 3490–3497.
- [39] R. Su, R. Tiruvalam, Q. He, N. Dimitratos, L. Kesavan, C. Hammond, J.A. Lopez-Sanchez, R. Bechstein, C.J. Kiely, G.J. Hutchings, F. Besenbacher, Promotion of phenol photodecomposition over TiO₂ using Au, Pd, and Au–Pd nanoparticles, *ACS Nano* 6 (2012) 6284–6292.
- [40] X. Li, J.-L. Shi, H. Hao, X. Lang, Visible light-induced selective oxidation of alcohols with air by dye-sensitized TiO₂ photocatalysis, *Appl. Catal. B* 232 (2018) 260–267.
- [41] Y. Li, P. Ren, D. Zhang, W. Qiao, D. Wang, X. Yang, X. Wen, M.H. Rummeli, H. Niemantsverdriet, J.P. Lewis, F. Besenbacher, H. Xiang, Y. Li, R. Su, Rationally designed metal cocatalyst for selective photosynthesis of bibenzyls via dehalogenative C–C homocoupling, *ACS Catal.* 11 (2021) 4338–4348.
- [42] J. Yu, Q. Liu, W. Qiao, D. Lv, Y. Li, C. Liu, Y. Yu, Y. Li, H. Niemantsverdriet, B. Zhang, R. Su, Catalytic role of metal nanoparticles in selectivity control over photodehydrogenative coupling of primary amines to imines and secondary amines, *ACS Catal.* 11 (2021) 6656–6661.
- [43] Y. Shiraiishi, K. Fujiwara, Y. Sugano, S. Ichikawa, T. Hirai, N-monoalkylation of amines with alcohols by tandem photocatalytic and catalytic reactions on TiO₂ loaded with Pd nanoparticles, *ACS Catal.* 3 (2013) 312–320.
- [44] J. Greeley, T.F. Jaramillo, J. Bonde, I. Chorkendorff, J.K. Nørskov, Computational high-throughput screening of electrocatalytic materials for hydrogen evolution, *Nat. Mater.* 5 (2006) 909–913.
- [45] D. Lv, Y. Lei, D. Zhang, X. Song, Y.-W. Li, J.W.H. Niemantsverdriet, W. Hao, Y. Deng, R. Su, Effect of Pd and Au on hydrogen abstraction and C–C cleavage in photocatalytic conversion of glycerol: beyond charge separation, *J. Phys. Chem. C* 124 (2020) 20320–20327.
- [46] C. Li, X. Wang, A. Cheruvathur, Y. Shen, H.-W. Xiang, Y.-W. Li, H. Niemantsverdriet, R. Su, In-situ probing photocatalytic C–C bond cleavage in ethylene glycol under ambient conditions and the effect of metal cocatalyst, *J. Catal.* 365 (2018) 313–319.
- [47] VdA.M. Kraan, R.C.H. Nonnekens, F. Stoop, J.W. Niemantsverdriet, Characterization of FeRu/TiO₂ and Fe/TiO₂ catalysts after reduction and Fischer-Tropsch synthesis by Mossbauer spectroscopy, *Appl. Catal.* 27 (1986) 285–298.
- [48] H. Song, X. Meng, Z.-j Wang, Z. Wang, H. Chen, Y. Weng, F. Ichihara, M. Oshikiri, T. Kako, J. Ye, Visible-light-mediated methane activation for steam methane reforming under mild conditions: a case study of Rh/TiO₂ catalysts, *ACS Catal.* 8 (2018) 7556–7565.
- [49] N.O. Balayeva, Z. Mamiyev, R. Dillert, N. Zheng, D.W. Bahnemann, Rh/TiO₂-photocatalyzed acceptorless dehydrogenation of n-heterocycles upon visible-light illumination, *ACS Catal.* 10 (2020) 5542–5553.
- [50] T. Wang, S. Wang, Q. Luo, Y.-W. Li, J. Wang, M. Beller, H. Jiao, Hydrogen adsorption structures and energetics on iron surfaces at high coverage, *J. Phys. Chem. C* 118 (2014) 4181–4188.
- [51] M. Mavrikakis, J. Rempel, J. Greeley, L.B. Hansen, J.K. Nørskov, Atomic and molecular adsorption on Rh(111), *J. Chem. Phys.* 117 (2002) 6737–6744.
- [52] B. Erdem, R.A. Hunsicker, G.W. Simmons, E.D. Sudol, V.L. Dimonie, M.S. El-Aasser, XPS and FTIR Surface characterization of TiO₂ particles used in polymer encapsulation, *Langmuir* 17 (2001) 2664–2669.